2021

Thermodynamic Investigation and Design Concept of a bi-directional Wankel Machine for Compression and Expansion in Natural Gas Storage and Distribution Applications

Thomas Werner Moesch
Technische Universität Dresden, Germany, thomas.moesch@tu-dresden.de

Konrad Klotsche

Gotthard Will

Christiane Thomas

Ullrich Hesse

Thermodynamic investigation and design concept of a bi-directional Wankel machine for compression and expansion for natural gas storage and distribution applications

Thomas W. MOESCH*, Konrad KLOTSCHE, Gotthard WILL, Christiane THOMAS, Ullrich HESSE

Technische Universität Dresden,
Institute of Power Engineering,
Bitzer-Chair of Refrigeration, Cryogenics and Compressor Technology
Dresden, Germany
thomas.moesch@tu-dresden.de

* Corresponding Author

ABSTRACT

The distribution and storage of natural gas is based on different pressure levels. The pressure is increased by process gas compressors and currently reduced by throttling valves. The isenthalpic throttling leads to exergy losses. As part of an industry project the TU Dresden and the IME Aachen GmbH developed a bi-directional Wankel machine that may be used for both compression and expansion and thus recover some of the exergy losses. The Wankel machine uses rotary valves for suction and discharge control with fixed opening and closing angles in regards to the displacer rotation. This study shows the detailed design concept of the Wankel machine and the corresponding thermodynamic model, which is based on the compressor calculation software KVA developed at the TU Dresden. The model and its results were used to conduct an in-depth analysis of the machine, including pressures and temperature curves during one displacer rotation, its expected overall efficiencies, occurring exergy losses and its economic potential. The results reveal a considerable energy savings potential for future natural gas storage and distribution application.

1. INTRODUCTION

There is a vast network of pipelines for the distribution of natural gas in Germany. Natural gas is typically stored at pressures up to 30 MPa. The gauge pressures in the transfer lines differs (e.g. long distant transfer lines vs. local distribution lines) and may reach values up to 12 MPa in high-pressure lines, up to 0.1 MPa in medium-pressure lines and up to 0.01 MPa in low-pressure lines (Adler *et al.* 2014). The pressure is reduced and/or elevated (e.g. for biogas injection) at gas transfer stations to match the previous or subsequent lines. Currently, the pressure reduction is achieved by throttling the gas, which then needs to be preheated due to the resulting Joule-Thomson effect. Möller *et al.* (2004) suggest the usage of an expansion machine for pressure reduction and a combined heat and power unit for preheating, which would lead to low CO_2 emissions for the power generation of 0.3 t_{CO_2}/MWh_{el} as compared to Germany's current CO_2 emission coefficient of 0.474 t_{CO_2}/MWh_{el} (Icha and Kuhs, 2019). Mischner *et al*. (2019) suggest the usage of a heat pump for preheating and an expansion machine as a power source for the heat pump compressor. One option for the expansion machine is a Wankel expander. Wankel machines were mainly applied as combustion engines (Yamamoto, 1981). However, applications as compressor machines and expander machines have shown to be equally appealing by recent publications of Garside (2017) and Francesconi *et al.* (2017).
This paper proposes a prototype Wankel type machine design based on a patent (Schaarschmidt and Lenth, 2016), which aims to combine both compression and expansion process in one machine by simply changing its direction of rotation. The paper includes an in-depth thermodynamic investigation of this machine for its rating conditions. The investigation is based on the in-house calculation software called KVA (Hesse and Will, 2014), which was modified for a Wankel type machine. The model is thoroughly described and its results are used to conduct an exergy loss analysis and a profitability analysis.

2. DESIGN CONCEPT

The Wankel machine is based on a 2:3 trochoid geometry and it is designed for an operation with dry natural gas (methane) and operating conditions for the compression mode as shown in Table 1.

Table 1: Operating conditions for compression mode

Parameter	**Value**	**Unit**
Low pressure	0.6	MPa (abs.)
High pressure	1.3	MPa (abs.)
Suction temperature	283.15	K
Standard volume flow (T = 283 K, p = 0.1013 MPa)	1300	m³/h
Shaft speed	50	1/s

2.1 Geometry and components

The assembly of the machine and its main components are shown in Figure 1. Both bearings and gas seals are not shown here, however, they are included in the final machine design, which is based on Wankel type engines (Yamamoto, 1981). The geometry of the compressor housing bore is based on a trochoid curve with a base radius r_B an eccentricity e. The curve is defined in a Cartesian system by the following equation.

$$\begin{pmatrix} x \\ y \end{pmatrix}_{\text{Housing}} = \begin{pmatrix} e\cos(\varphi) + r_B \cos(\varphi/3) \\ e\sin(\varphi) + r_B \sin(\varphi/3) \end{pmatrix} \tag{1}$$

The rotor flanks are based on a circle approach with a radius r_R. Each rotor segment is defined by equation (2).

$$\begin{pmatrix} x \\ y \end{pmatrix}_{RotSeg,i} = \begin{pmatrix} r_{off}\cos(\varphi_{off,i}) + r_R \cos(\varphi_i) \\ r_{off}\sin(\varphi_{off,i}) + r_R \sin(\varphi_i) \end{pmatrix} \tag{2}$$

$$\text{with } \varphi_{off,i} = \begin{cases} \pi & \text{for } i = 1 \\ -\pi/3 & \text{for } i = 2 \\ \pi/3 & \text{for } i = 3 \end{cases} \quad \text{and} \quad \varphi_i = \begin{cases} -\alpha \ldots \alpha & \text{for } i = 1 \\ -\alpha + 2\pi/3 \ldots \alpha + 2\pi/3 & \text{for } i = 2 \\ -\alpha - 2\pi/3 \ldots \alpha - 2\pi/3 & \text{for } i = 3 \end{cases}$$

The offset of the circle centers to the rotor center r_{off} and the opening angle of the circle segments α are defined by equations (3) and (4).

$$r_{off} = r_R \cos(\alpha) - r_B \cos(\pi/3) \tag{3}$$

$$\alpha = 2\arcsin\left(\frac{r_B}{r_R}\sin(\pi/3)\right) \tag{4}$$

All geometry parameters for the Wankel machine are summarized in Table 2.

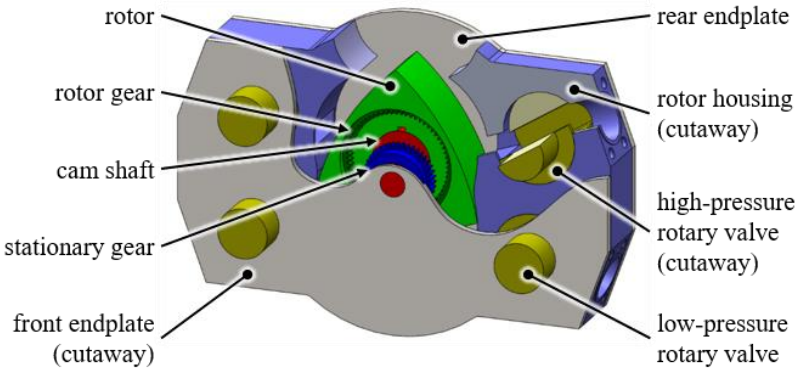

Figure 1: Wankel machine design 3D cutaway view

Table 2: Geometry parameters

Parameter	Value	Unit
Base radius r_B	120	mm
Eccentricity e	24	mm
Rotor flank radius r_R	456	mm
Offset of the circle centers to the rotor r_{off}	384	mm
Opening angle of the circle segments α	26.35	°
Outer diameter of rotary valve	104	mm
Size of flow port in low-pressure rotary valves (height x width)	62.5 x 67.5	mm
Size of flow port in high-pressure rotary valves (height x width)	62.5 x 36.0	mm
Size of flow ports between rotary valves and working chambers (height x width)	62.5 x 26.0	mm
Rotor height	72.5	mm

2.2 Mode of operation

The rotor is coupled by the cam shaft, but its rotating movement is set by its rotor gear and the stationary gear in the housing cover with a gear ratio of 2:3. This leads to a transmission of 3:1 between shaft and rotor. The rotary valves are connected to the shaft via drive belt with a transmission of 2:1. The trochoid rotor and the trochoid-shaped cylinder bore form up to six working chambers which lead to six individual suction, compression and discharge processes during one rotor rotation. Figure 2 shows the Wankel machine at different rotor angles and highlights one of its working chambers (WC11). Figure 3 shows the resulting volume curve of the two working chambers WC11 and WC12 and the opening area curves for the corresponding high-pressure and low-pressure rotary valves. The curves for volumes of WC21/WC22 and WC31/WC32 and their corresponding rotary valve opening areas are identical to the shown curves with an offset in the rotor angle of +240° and +120°, respectively. The resulting swept volume per working chamber is 1200 cm³. The compression mode and expansion mode only differ in their direction of rotation and the mirrored opening curves of the rotary valves (see Figure 3). The rotary valves control the timing and duration of the suction/discharge process and set the built-in compression and expansion ratio ($\Psi_C = \Psi_E = 1.85$). The rotor angles in Figure 2 show the points of opening and closing of the lower low-pressure rotary valve ($\varphi_{R,lrvo}$ = 105°, $\varphi_{R,lrvc}$ = 180°) and the high-pressure rotary valve ($\varphi_{R,hrvo}$ = 225° $\varphi_{R,hrvc}$ = 273°) during compression mode.

$$\Psi_C = V_{\mathrm{lrvc}} / V_{\mathrm{hrvo}} \qquad \Psi_E = V_{\mathrm{lrvo}} / V_{\mathrm{hrvc}} \tag{5}$$

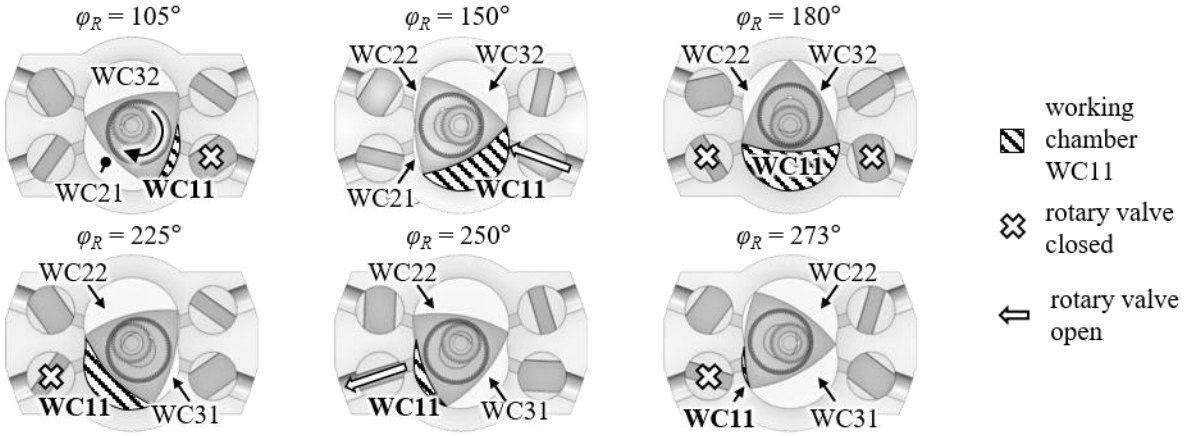

Figure 2: Wankel machine and working chambers (WC) at different rotor positions in compression mode

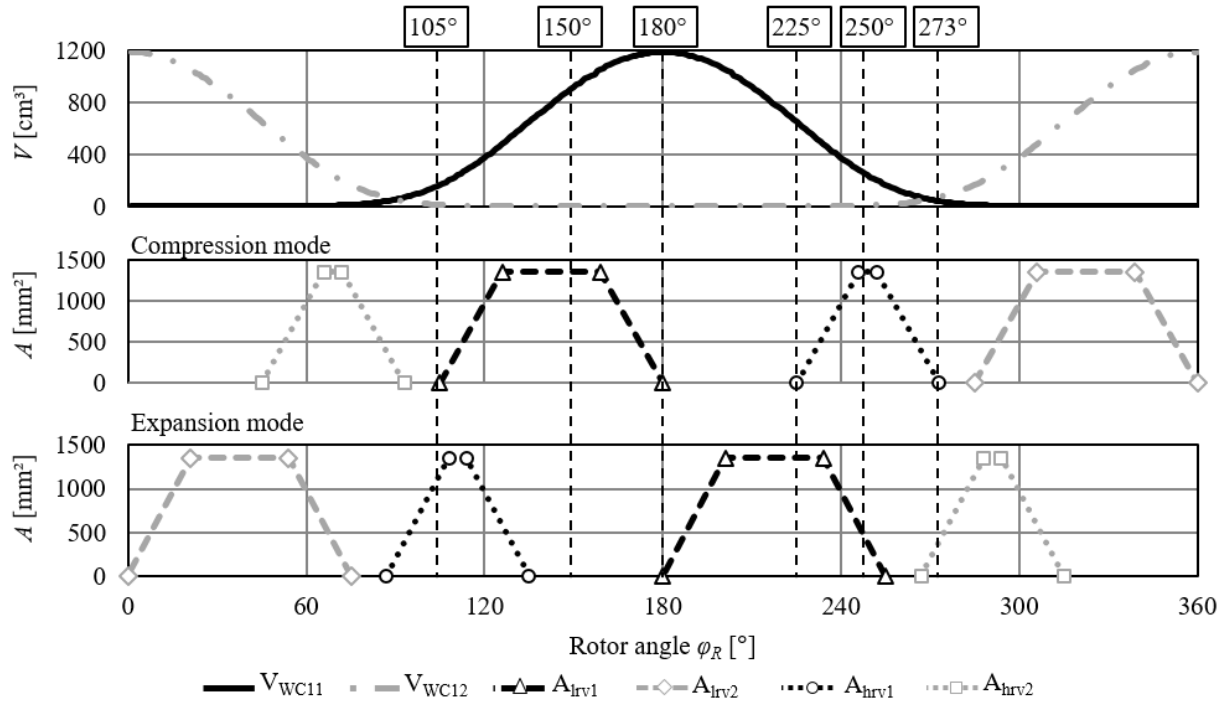

Figure 3: Volume curve of the working chambers WC11 and WC12 and the corresponding opening area curves of the high-pressure rotary valves (hrv1, hrv2) and the low-pressure rotary valves (lrv1, lrv2)

3. THERMODYNAMIC MODEL

The goal of the calculation is the determination of all relevant thermodynamic parameters of the working fluid within the Wankel machine. The calculations are carried out with an in-house program, called KVA, which computes the thermodynamic steady state of the fluid based on a 0-dimensional approach. Hesse and Will (2014) gave a detailed description of the calculation program. Klotsche *et al.* (2018) applied KVA for the first time to a Wankel machine as a household refrigerator compressor. The calculation itself requires a model of the Wankel machine, which includes all relevant volumes (working chambers, suction and pressure chambers, *etc.*) and their junctions each represented by connecting elements. This composes a network of all relevant gas-containing components. The volumes may be divided into four categories (see Table 3).

Table 3: Overview of different categories of volumes and their main properties

Category	Temperature	Pressure	Volume	Typical example
Type 1	constant	constant	constant	Suction boundary condition
Type 2	*variable*	constant	constant	Discharge boundary condition
Type 3	*variable*	*variable*	constant	Suction & discharge chamber
Type 4	*variable*	*variable*	*variable*	Working chamber

There are five different types of connection elements available, including valves, pipes, cross-sectional constrictions (which can be constant over time or time-controlled, *i.e.* controlled by edges), gaskets, and heat exchangers. The heat rejection of the Wankel machine is realized by wall elements that can be modelled to absorb, store and release heat from the gas contained in the volumes to and from the environment. Wall elements require defined contact surfaces, heat conduction properties as well as the geometric properties. The changes of state and mass in the volumes result from the properties of surrounding components, in particular the temporal behavior of the working chamber volumes, as well as the properties of the connecting elements and the given boundary conditions, *i.e.* the low- and high-pressure interface to the connected system or cycle. During the calculations, both gas pressure and gas temperatures of all volumes are determined for each time step. All other relevant thermodynamic parameters are derived from *p* and *T*.

The governing equations are based on the first law of thermodynamics and the ideal gas equation, shown by Hesse and Will (2014).

$$\frac{1}{p}\frac{dp}{dt} = \frac{K}{K-1}\cdot\left(\frac{p}{mKRT}\frac{dQ}{dt} - \frac{1}{V}\frac{dV}{dt} - \frac{1}{K}\frac{dK}{dt}\right) \tag{6}$$

$$\frac{1}{T}\frac{dT}{dt} = \frac{K}{K-1}\cdot\left(\frac{p}{mKRT}\frac{dQ}{dt} - \frac{1}{VK}\frac{dV}{dt} - \frac{1}{K}\frac{dK}{dt}\right) - \frac{1}{m}\frac{dm}{dt} - \frac{1}{R}\frac{dR}{dt} \tag{7}$$

All parameters can be found in the list of symbols, the parameters R and K are defined as followed:

$$R = \frac{p}{\rho T} \qquad\qquad K = \frac{h}{RT} \tag{8}$$

The temporal changes in pressure and temperature of all volume elements are calculated with a time-stepping method. Hesse and Will (2014) provided information about this procedure. Figure 4 shows a 2D cutaway of the Wankel design with volume and connecting elements for this time step. Figure 5 shows the corresponding calculation model with all volume and connecting elements and one wall element. Note that upper and lower-case acronyms represent volume and connecting elements, respectively. The model comprises six working chambers (WC11 – WC32) that are created between the displacer and the housing (cylinder and end plates) over one complete displacer rotation and both low- and high-pressure supply lines in the upper and lower machine part. The following list represents every volume and connecting element starting from the system interface to the working chamber (the first letter shows the pressure level: l or L = low-pressure, h or H = high-pressure):

- a low- or high-pressure line (ll1/ ll2 or hl1/ hl2) representing the pipe between the Wankel machine and the connected circuit, *i.e.* the boundary conditions of the model (L, H) (not shown in Figure 4)
- a damping volume (LDV1/ LDV2 or HDV1/ HDV2) (not shown in Figure 4)
- a rotary valve (lrv1/ lrv2 or hrv1/ hrv2)
- a valve chamber (LVC1/ LVC2 or HVC1/ HVC2),
- and six time-controlled flow ports (lfp11 – lfp16/ lfp21 – lfp26 or hfp11 – hfp16/ hfp21 – hfp26) acting as a link between the valve chamber with each of the working chambers time-dependently. Each valve chamber temporarily connects with each working chamber during one complete rotation of the displacer.

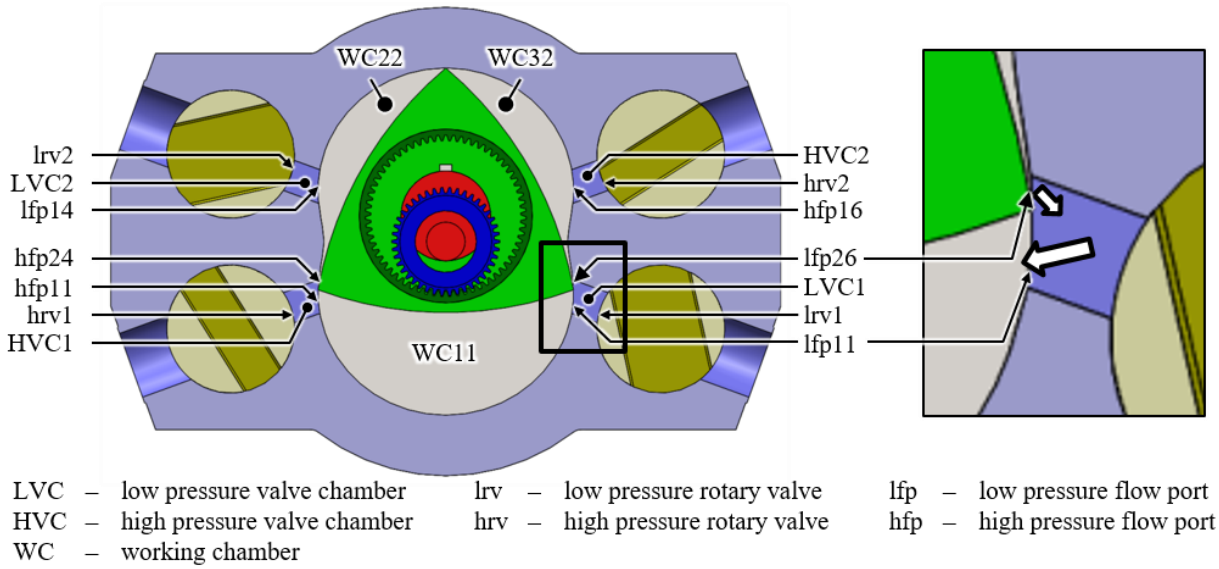

Figure 4: 2D-cutaway of Wankel design with volume elements and connecting elements

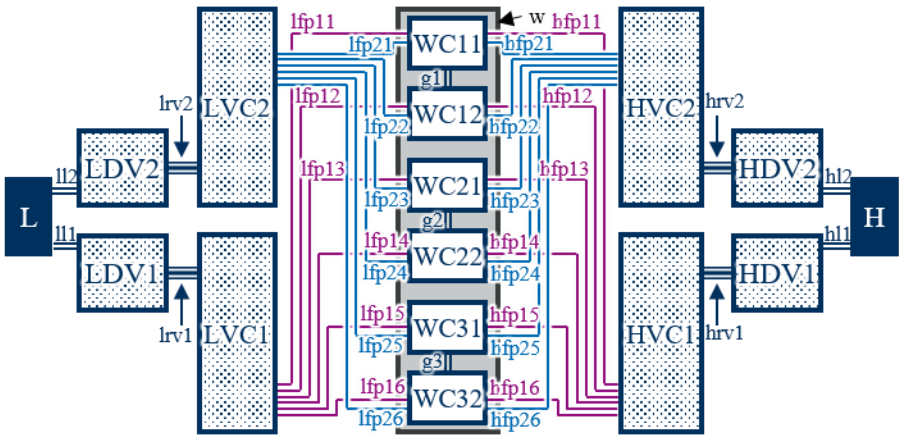

Figure 5: KVA model for the Wankel machine

The connecting elements g1 – g3 are gaps with a constant cross-section. They represent the leakage gap between the cylinder cusps and the moving displacer flank, which connects consecutive working chambers (*e.g.* WC11 and WC12). The wall element w accounts for the heat transfer between the working chambers and the environment. The flow through the connecting elements flow ports (lfp, hfp), rotary-valve (lrv, hrv), and leakage gaps (g) is based on an isentropic nozzle flow for compressible gases (Jobsen, 1955).

$$\dot{m} = A \cdot \mu \cdot \psi\left(p_1/p_2, \kappa\right) \cdot \sqrt{2\rho_1 p_1} \tag{9}$$

$$\text{with} \quad \psi\left(p_2/p_1, \kappa\right) = \begin{cases} \left(\frac{2}{\kappa+1}\right)^{\frac{1}{\kappa+1}} \cdot \sqrt{\frac{\kappa}{\kappa+1}} & \text{for} \quad p_2/p_1 \le \left(\frac{2}{\kappa+1}\right)^{\frac{\kappa}{\kappa-1}} \\ \sqrt{\frac{\kappa}{\kappa-1} \cdot \left[\left(p_2/p_1\right)^{\frac{2}{\kappa}} - \left(p_2/p_1\right)^{\frac{\kappa+1}{\kappa}}\right]} & \text{for} \quad \left(\frac{2}{\kappa+1}\right)^{\frac{\kappa}{\kappa-1}} < p_2/p_1 < 1 \end{cases}$$

Where A is the cross-sectional flow area, μ is the flow coefficient that takes friction losses into account, κ is the isentropic exponent, p_1 is the pressure at the inlet, p_2 is the pressure at the outlet, ρ_1 is the density at the inlet.

4. SIMULATION RESULTS

The calculation model is used to conduct a detailed analysis for both compression and expansion mode. The investigated operating point is similar to the operating conditions in Table 1 with an ambient temperature of 300 K. However, the expansion mode was simulated for a different inlet temperature (T = 318 K) than the compression mode (T = 283 K) to account for a preheating of the gas prior to expansion. The main results are summarized in Table 3. The results show that the machine slightly exceeds the volume flow demands of the operating conditions and achieves relatively similar exergetic efficiencies for both compression and expansion mode even though the compressor mode has a lower volumetric efficiency. The following sub-sections reveal a detailed analysis of the simulation results.

Table 3: Summarized simulation results for compression and expansion mode

Parameter	**compression mode**	**expansion mode**
Volume flow [m³/h] (T = 283 K, p = 0.1013 MPa)	1473	1885
Power input [kW]	45.1	-29.9
Volumetric efficiency [%]	57.2	75.1
Isentropic efficiency [%]	75.3	69.4
Exergetic efficiency [%]	79.5	75.1

4.1 Analysis of pressure and temperature curves

Figure 6 shows the resulting pressure and temperature curves for chamber WC11 and its connected volumes during compression and expansion mode.

The high-pressure peak during compression mode at φ_R = 236° indicates a valve pressure loss up to 0.18 MPa due to an insufficient valve opening area. The rising temperature and pressure in the the low-pressure rotary valve chamber (LVC1) starting at φ_R = 273° shows the compression of the remaining gas in WC11 and then its re-expansion in WC12 after the high-pressure rotary valve (hrv1) closed while the low-pressure rotary valve (lrv2) has not yet opened (see Figure 2, φ_R = 273°).

For the expansion mode, the pressure minimum in the high-pressure valve chamber (at φ_R = 51°) indicates under-expansion and recompression losses due to late control valve opening. The pressure drop during the admission starting at φ_R = 90° indicates a restricted flow into the working chamber caused by a small high-pressure rotary valve opening area during admission. The working chamber pressure decreases below the low-pressure level at φ_R = 160° which indicates a late opening of the low-pressure rotary valve and results in under-expansion losses. During this under-expansion the gas reaches temperatures below 283 K (T_{min} = 274 K at φ_R = 170°) which may lead to condensation within the machine in case of remaining moisture content in the natural gas. However, the recompression of the gas (starting at φ_R = 175°) leads to minimum gas temperatures of T_{LVC} = 283 K in the low-pressure valve chamber and T_{LDV} = 285 K in the low-pressure damping volumes. Therefore, there is no need for additional reheating of the discharged gas.

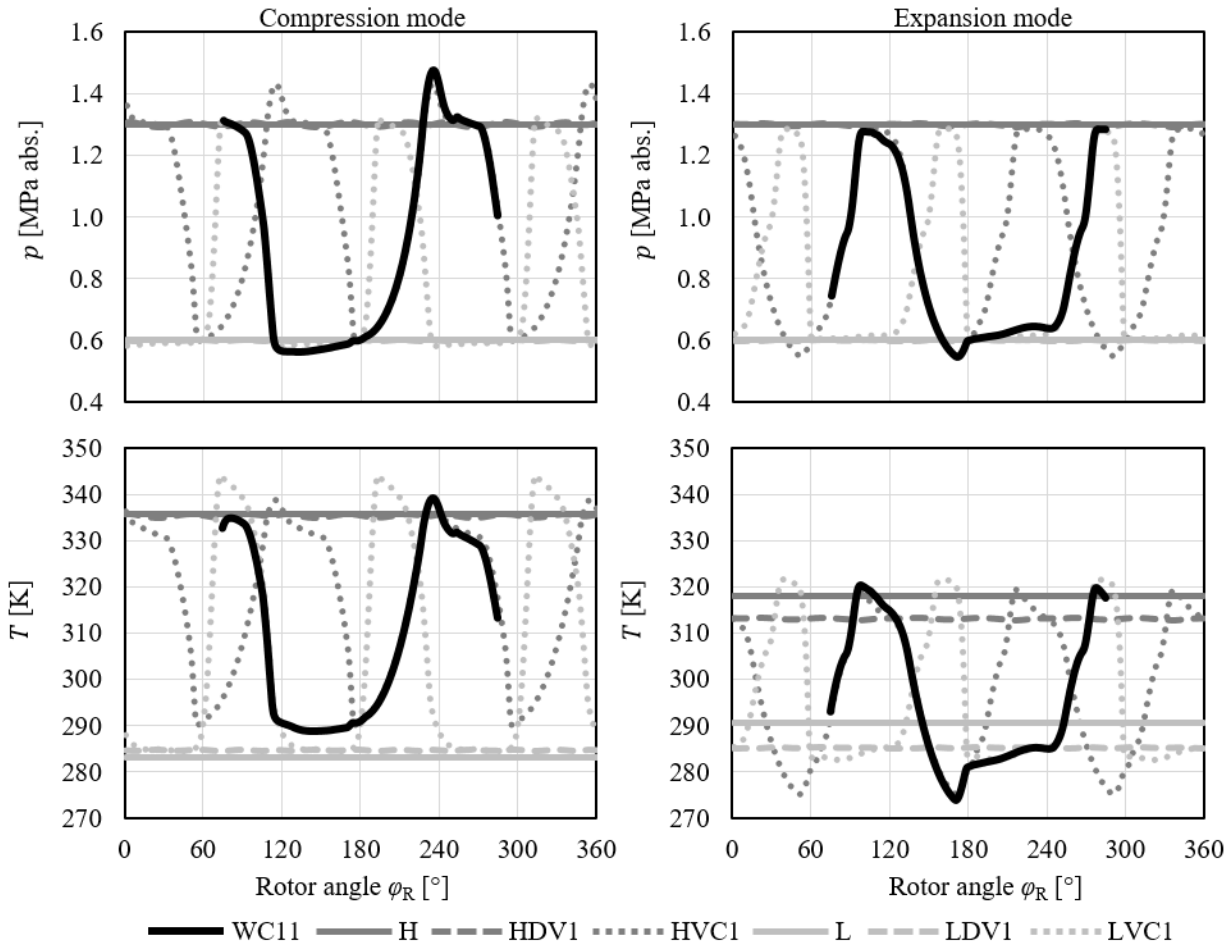

Figure 6: Pressure and temperature curves for working chamber WC11 and its connected volumes

4.2 Exergy flow loss analysis

The temperature and pressure curves only allow an evaluation of the change in state in all volumes. For a more detailed loss analysis, the exergy losses of each component are evaluated. The exergy flow loss analysis is based on the general exergy flow balance as proposed by Kretzschmar and Kraft (2016). Both potential and kinetic energy terms are neglected.

$$\dot{E}_{loss12} = \dot{E}_{\dot{Q}12} + P_{t12} + P_{diss12} - \left(\Sigma\dot{E}_2 - \Sigma\dot{E}_1\right) \tag{10}$$

with $\dot{E}_{\dot{Q}12} = \sum_i \frac{T_i - T_{amb}}{T_i}\dot{Q}_i$ $P_{t12} = \dot{m}\int_{p_1}^{p_2} v(p)\,dp$ $\dot{E} = \dot{m}\cdot\left[h - h_{amb} - T_{amb}\cdot\left(s - s_{amb}\right)\right]$

Where $\dot{E}_{\dot{Q}12}$ is the exergy flow loss due to heat exchange, P_{t12} is the added mechanical power to the flow, P_{Diss12} is the dissipated mechanical power through friction and $\dot{E}_2$ and $\dot{E}_1$ are the exergy flows of the entering and leaving fluid, respectively.

The results of the loss analysis are shown in Figure 7. The upper diagrams distinguish between *Working Chambers (WCs)* which account for all working chambers (WC11 to WC32), *Volumes* which account for all fixed-volume chambers (DV and VC), *Ports* which include all variable flow port openings (lfp11 to hfp26), *Valves* which include all rotary valves (lrv1 to hrv2), and *Pipes* which include both low-pressure and high-pressure lines (ll1 to hl2). The lower diagrams distinguish between *"A"-*, *"B"-*, and *"C"-ports*. *"A"-ports* include all ports that connect the working chambers with the intended low-pressure and high-pressure valve chambers (lfp11, lfp13, lfp15, lfp22, lfp24, lfp26, hfp11, hfp13, hfp15, hfp22, hfp24, hfp26). *"B"-ports* include all ports that lead to an unintentional connection between working chambers and valve chambers (lfp12, lfp14, lfp16, lfp21, lfp23, lfp25, hfp12, hfp14, hfp16, hfp21, hfp23, hfp25). "*C"-ports* include the non-sealed gap between consecutive working chambers (g1 to g3).

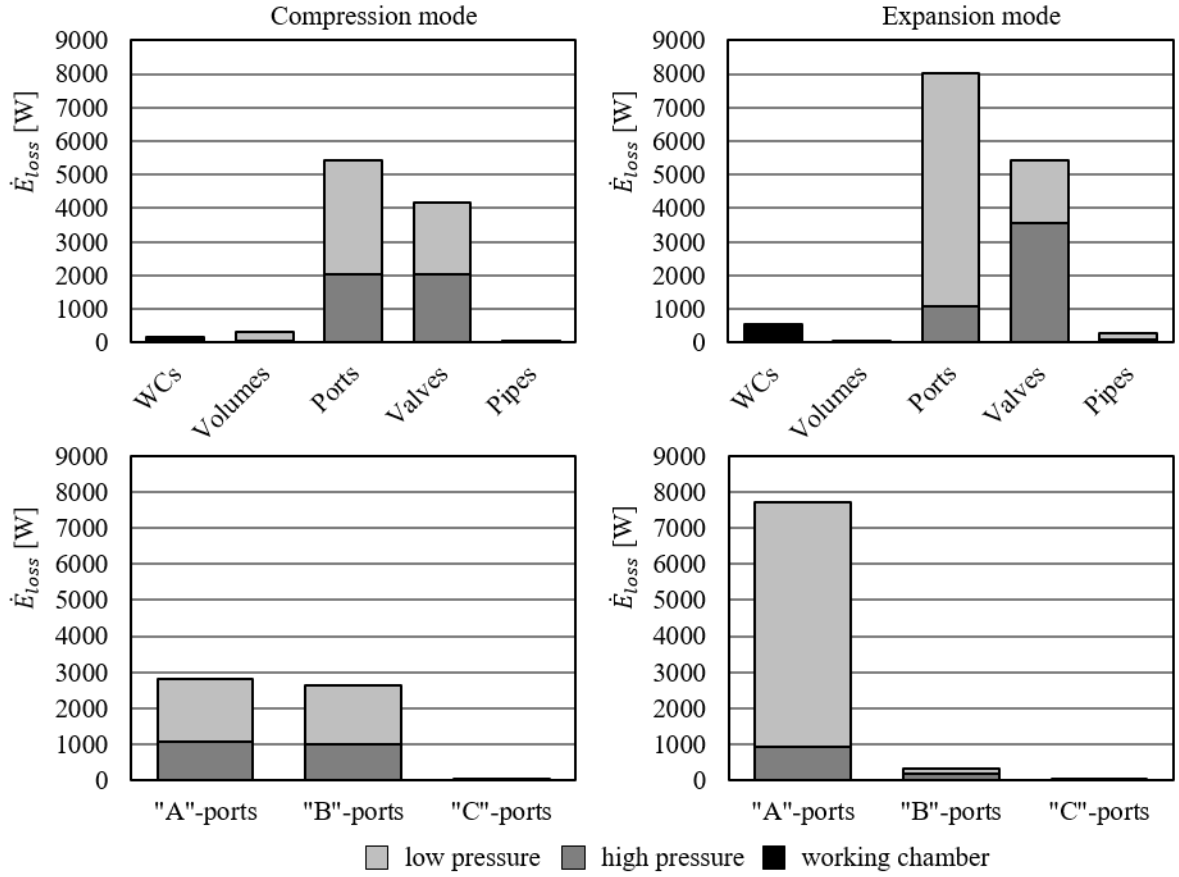

Figure 7: Exergy flow losses (by component type) during compression and expansion mode

The main exergy flow losses during compression mode occur in the low-pressure ports with $\sum \dot{E}_{loss,lfp}$= 3390 W followed by the low-pressure and high-pressure rotary valves and high-pressure ports with $\sum \dot{E}_{loss,lrv}$ = 2120 W, $\sum \dot{E}_{loss,hrv}$ = 2050 W, and $\sum \dot{E}_{loss,hfp}$ = 2040 W. These coincide with the pressure losses due to the limited size of the ports and the fixed opening phase of the rotary valves.
The main exergy flow losses during expansion mode occur in the low-pressure ports with $\sum \dot{E}_{loss,lfp}$ = 6810 W and the high-pressure valves with $\sum \dot{E}_{loss,hrv}$ = 3560 W. This coincides with both the steep pressure increase during the discharge and the pressure loss during the suction process. It ultimately shows that the opening phase of the high-pressure rotary valve and the sizing of the low-pressure ports are not ideal for the expansion mode. The leakage paths g1 through g3 only have a minimal effect on the overall exergy losses.
The exergy loss analysis shows higher exergy losses through high-pressure rotary valves during expansion mode as compared to compression mode and a significant difference in the impact of the ports. This shows the importance of the rotary valve and port design and its compromise by optimization the fixed opening and closing angles for both compression and expansion mode and reducing the overall exergy losses instead of finding the optimal design for only one mode. Future machine designs need to apply more variable rotary valve configurations

4.3 Profitability analysis

The usable electric power during the expansion mode and its economic benefit depend on the initial gas temperature, the preheating method (boiler or heat pump) and the generator efficiency. The additional preheating capacity for the calculated expansion mode volume flow can be approximated to be 27.4 kW when assuming an initial gas temperature of 283.15 K and dry natural gas with a high methane content (>93%) and a specific heat capacity of c_p = 2.23 kJ/(kg·K). For a comparison of both boiler and heat pump method, the following assumptions were applied:

- each generator efficiency and boiler efficiency equals 0.95,
- CO_2 emission factor is 0.2 t_{CO_2}/MWh for natural gas, 0.471 t_{CO_2}/MWh for electricity (Icha and Kuhs, 2019),
- the air/gas heat pump has a *SEER* of 2.5,
- yearly operating time is 6130 h (degree of utilization = 70%),
- costs of gas is 0.06 Euro/kWh and costs of electricity is 0.30 Euro/kWh.

The results are summarized in Table 4 and show that Method 1 leads to a higher electric power output and a higher economic potential. However, Method 2 does not cause any CO_2 emission and requires no natural gas consumption and is therefore the better option for a future carbon-neutral industry.

Table 4: Results of ecological and economic potential analysis for one unit

Parameter	**Method 1 (boiler preheater)**	**Method 2 (heat pump preheater)**
Usable electric power output [MWh/a]	174.2	107.0
Required natural gas [MWh/a]	176.8	0
CO_2 emission factor [kg_{CO_2}/kWh]	0.20	≈ 0
Avoided CO_2 emission [t_{CO_2}/a]	**46.7**	**50.4**
Money savings [Euro/a]	**41,648**	**32,103**

6. CONCLUSIONS

The proposed Wankel machine design allows a bi-directional operation as compressor and expander. The different operating modes (compression and expansion) were achieved by using actuated rotary valves for both inlet and outlet. The compression and expansion of natural gas with current Wankel machine design leads to isentropic efficiencies of 75.3 % / 69.4 % and volumetric efficiencies of 57.2 % / 75.1 % respectively. The largest exergy occur at the ports and the rotary valves and are particularly significant in the low-pressure ports during expansion mode. The expansion mode allows a total energy savings of 107.0 kWh/a when combined with a heat pump (with *SEER* = 2.5) as a gas preheater and 174.2 MWh/a by using a boiler preheater but with a CO_2 emission factor of 0.20 kg_{CO_2}/ kWh.

NOMENCLATURE

A	area	[m²]	R	real gas parameter (see Eq. 7)	[J·kg^{-1}·K^{-1}]
d	diameter	[m]	s	specific entropy	[J·kg^{-1}·K^{-1}]
c_p	specific heat capacity	[J·kg^{-1}·K^{-1}]	$SEER$	seasonal energy efficiency ratio	[1]
e	eccentricity	[m]	T	temperature	[K]
$\dot{E}$	exergy flow	[W]	v	specific volume	[m³/kg]
h	specific enthalpy	[J/kg]	V	volume	[m³]
K	real gas parameter (see Eq. 7)	[1]	w	width	[m]
m	mass	[kg]	x, y	Cartesian coordinates	[m]
$\dot{m}$	mass flow rate	[kg/s]	α	segment angle	[rad]
Q	heat	[J]	η	efficiency	[1]
$\dot{Q}$	heat flow	[W]	κ	isentropic exponent	[1]
p	pressure	[Pa]	μ	flow coefficient	[1]
P	power	[W]	φ	angle	[rad]
r	radius	[m]	$\Psi_{C\|E}$	compression | expansion ratio	[1]

Subscript

amb	ambient	*i*	index of element	*off*	offset
B	base	*lfp*	low-pressure flow port	*R*	rotor
diss	dissipated	*lrv*	low-pressure rotary valve	*t*	mechanical
hrv	high-pressure rotary valve	*lrvo|c*	*lrv* opens | just closed	*WC*	working chamber
hrvo|c	*hrv* opens | just closed	*min*	minimum		

REFERENCES

Adler, P., Billig, E., Brosowski, A., Daniel-Gromke, J., Falke, I., Fischer, E., Grope, J., Holzhammer, U., Postel, J., Schnutenhaus, J., Stecher, K., Szomszed, G., Trommler, M., Urban, W. (2014). *Leitfaden: Biogasaufbereitung und –einspeisung*. Fachagentur Nachwachsende Rohstoffe e.V. (FNR)

Francesconi, M., Caposciutti, G., & Antonelli, M. (2017). An experimental and numerical analysis of the performances of a Wankel steam expander. *Energy Procedia*, *129*, 395-402.

Garside, D. W. (2017). A new Wankel-type compressor and vacuum pump. In *IOP Conference Series: Materials Science and Engineering* (Vol. 232, No. 1, p. 012065). IOP Publishing.

Hesse, U., & Will, G. (2014). Thermodynamic Calculation of Reciprocating Compressors Plants. *Proceedings of the 9th Conference of the EFRC,* Vienna, Austria (158-168).

Icha, P., & Kuhs, G. (2019). Entwicklung der spezifischen Kohlendioxid-Emissionen des deutschen Strommix in den Jahren 1990-2018. Dessau-Roßlau.

Jobson, D. A. (1955). On the flow of a compressible fluid through orifices. *Proceedings of the Institution of Mechanical Engineers*, *169*(1), 767-776.

Klotsche, K., Moesch, T. W., Will, G., & Hesse, U. (2018). Thermodynamic modelling of reciprocating and Wankel type compressor for household refrigerators. Purdue Compressor Conference 2018

Kretzschmar, H. J., & Kraft, I. (2016). *Kleine Formelsammlung Technische Thermodynamik*. Carl Hanser Verlag GmbH Co. KG.

Mischner, J., Stang, R., & Gebhard, A. (2019). Energiestrombilanzen von Anlagen zur Energierückgewinnung für die Gasvorwärmung in Gasdruckminderungsanlagen. Vulkan-Verlag GmbH.

Möller, A., Niehörster, C., & Otto, F. (2004). Strom aus der Gasleitung – Entspannungsanlagen. *Gas- und Wasserfach. Gas-Erdgas*, *145*(6), 337-340.

Schaarschmidt, G. & Lenth, B. (2016). EP3091176A1. Munich: European Patent Office.

Yamamoto, K. (1981). *Rotary engine*. Tokyo, Japan: Sankaido Company.